Available online at www.sciencedirect.com

SciVerse ScienceDirect

Ceramics International 38 (2012) 4437–4444

CERAMICS INTERNATIONAL

www.elsevier.com/locate/ceramint

Review paper

Comparison on photocatalytic degradation of gaseous formaldehyde by TiO_2, ZnO and their composite

Yichuan Liao, Changsheng Xie *, Yuan Liu, Hao Chen, Huayao Li, Jun Wu

State Key Laboratory of Material Processing and Die and Mold Technology, Nanomaterials and Smart Sensors Laboratory, Department of Materials Science and Engineering, Huazhong University of Science and Technology, Wuhan 430074, PR China

Received 21 August 2011; received in revised form 28 February 2012; accepted 6 March 2012
Available online 14 March 2012

Abstract

In order to compare the photocatalytic properties of TiO_2, ZnO and their composite in the gas phase pollutant environment, nanocomposite with different mole ratios of TiO_2/ZnO were designed to degrade gaseous formaldehyde. The results showed that the rate constant of TiO_2 for formaldehyde degradation was 0.05 min^{-1} which was two orders of magnitude larger than that of ZnO in our experiment. Through comprehensive analysis of UV–vis diffuse reflectance (UV–vis) spectra, photoluminescence spectra (PL) and energy band diagram, it was found that the differences of photocatalytic properties between ZnO and TiO_2 may mainly originate from the increased recombination of photoinduced charges in ZnO. The photocatalytic properties of TiO_2/ZnO composite for formaldehyde degradation were much worse than those of TiO_2, while better than those of ZnO. The addition of a small amount of ZnO weakened the photocatalytic properties of TiO_2. It may be attributed to that the recombination action of photoinduced electron–hole pairs in ZnO.

Keywords: TiO_2/ZnO; Gaseous formaldehyde; Photocatalytic physics; Photocatalytic chemistry; Composition effect

Contents

1. Introduction

People spend most of their time indoors, while indoor air pollution is one of the top risks to human health, which has been validated by The Environmental Protection Agency [1,2]. Fortunately, a lot of work has been conducted to solve this problem. Photocatalysis has been proved to be a promising method to remove gaseous pollutants [3–7]. To date, most photocatalysis studies with valuable results were based on TiO_2 and the modification of TiO_2 [8–13]. For example, Liu et al. prepared TiO_2 hydrosols with high activity for photocatalytic degradation of gaseous formaldehyde [14]. The N-doped TiO_2 achieved high degradation reactivity for gaseous acetaldehyde degradation under visible light irradiation [15]. The photocatalytic activity for formaldehyde degradation of N-doped TiO_2 was enhanced markedly after being modified with NH_4F

* Corresponding author. Tel.: +86 27 8755 9835.
E-mail address: csxie@mail.hust.edu.cn (C. Xie).

0272-8842/$36.00
doi:10.1016/j.ceramint.2012.03.016

[16]. As a semiconductor material, the band gap (E_g) of ZnO is close to that of TiO_2 [17]. Some research groups reported the excellent photocatalytic property of ZnO in liquid pollutants [18–25]. Also, it is reported that the photocatalytic properties of TiO_2 and ZnO are very different in liquid [26–29]. However, little is well known about the photocatalytic effect of ZnO to degrade volatile organic compounds. Only Jing et al. compared the differences of deactivation and regeneration of ZnO and TiO_2 in the gas phase photocatalytic oxidation of n-C_7H_{16} and SO_2 [30]. Therefore, more investigations are needed to investigate the photocatalytic property of ZnO for gaseous pollutant degradation. Then how would their differences be in gas phase pollutant environment? It is also significant to explore the photocatalytic similarities and differences in gas between TiO_2 and ZnO from other viewpoints.

As we know, both generation and recombination of photoinduced electrons and holes are critical in photocatalysis [18,31,32]. In order to approach high photocatalytic efficiency, the recombination of photoinduced electrons and holes should be suppressed, thus enhance the photocatalytic efficiency of photocatalyst [33]. Specifically, some literatures pointed out that the compounding of different materials was a promising method to achieve efficient separation of photogenerated charges and to improve the catalytic activity of the photocatalysts [6,34–36]. For example, TiO_2/ZnO composite nanofibers exhibited much higher photocatalytic efficiency than pure TiO_2 nanofiber in degrading Rhodamine B and phenol molecules in water [37]. It is arisen the significance of comparing the photocatalytic degradation of gaseous pollutant by TiO_2, ZnO and their composite, as it will be helpful to understand their photocatalytic behavior in the gas phase.

In view of the issue mentioned above, nanocomposites with different mole ratios of TiO_2/ZnO were designed in this paper. Photocatalytic properties for gaseous formaldehyde degradation by TiO_2, ZnO and their composite films were presented. It would be worth stating that we try to compare the photocatalytic properties among TiO_2, ZnO and their composite from the two aspects of photocatalytic physics and photocatalytic chemistry. X-ray diffraction (XRD), field emission scanning electron microscopy (FE-SEM), UV–vis diffuse reflectance spectra (UV–vis DRS), and photoluminescence spectra (PL) were applied to investigate the phase structure, the grain morphology, the photocatalytic physical factors and the photocatalytic chemical factors of TiO_2, ZnO and their composite, respectively.

2. Experimental

2.1. Sample preparation

TiO_2 (Degussa P25, the average grain size: 30 nm), ZnO (the average grain size: 80 nm) and other chemicals used in the experiment were purchased of analytically pure grade without further purification. 11 ingredient points were designed with X_{ZnO} increasing from 0 to 1 by the interval of 0.1. Herein, X_{ZnO} denotes the mole fraction of ZnO in TiO_2/ZnO composite. A certain amount of organic solvent (with weight ratios of terpineol/butyl carbitol/dibutyl phthalate/ethyl-cellulose/span 85/di-n-butyl phthalate at 55:30:10:4:1) was added to TiO_2/ZnO powders. The organic solvent was totally dissolved at 100 °C for 3 h before adding. The weight ratios of TiO_2/organic and ZnO/organic solvent were 5:11 and 5:3, respectively. Ball milling (250 r/min, 3 h) was employed to mix them homogeneously, and the paste suitable for screen printing was obtained. Then, the paste was printed onto the alumina substrate by screen printing. The thickness of each film was controlled at 10 μm by the screen printing machine. The area of the quadrate film was 50 mm×50 mm. The design parameters of the sample were shown in Fig. 1. After laying aside at room temperature in the clean room environment for 12 h, the samples were sintered at 500 °C for 2 h in the air environment with heating rate of 1 °C/min, then was naturally cooled to room temperature in the furnace. In addition, organic solvent was also sintered at 500 °C for 2 h and it was found that the organic solvent was exhausted. Therefore, in the follow-up tests, the organic solvent did not exist in the samples. The more details of sample preparation could be referred to our previous work [38].

2.2. Degradation experiment and sample characterization

Formaldehyde (HCHO), as a typical indoor pollutant, exists widely in modern decorative materials, has been chosen as a model contaminant to evaluate the photocatalytic properties of materials. The degradation of gaseous formaldehyde was carried out in a photoelectrocatalytic (PEC) reactor system. The detailed descriptions of the PEC reactor system could be referred to our previous work [38]. The sample was set in a gas reaction chamber so that the whole photocatalytic film could be irradiated by a flat-type LED-light (365 ± 5 nm, 3.6 mW/cm^2). Formaldehyde gas held in a high pressure gas cylinder was fed to the reaction chamber and was absorbed by the solution of water and alcohol at the outlet. The concentration of gaseous formaldehyde in the chamber was detected on line with a Photoacoustic IR Multigas Monitor (Model 1412; INNOVA Air Tech Instruments). The gaseous formaldehyde was allowed to reach adsorption and desorption equilibrium for 30 min. After equilibrium, the initial concentration of formaldehyde in the chamber was about 50 ± 1 ppm (parts per million, 1 ppm = 40.9 μmol/m^3). Then, the LED light was on to irradiate the film. Each set of degradation experiment under LED irradiation lasted for 60 min. All the tests were performed at room temperature (25 °C) controlled by air-conditioner. Each

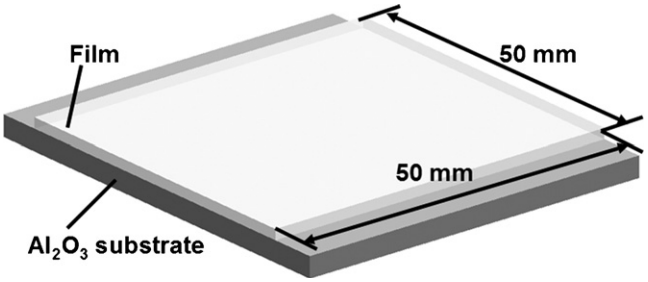

Fig. 1. Schematic diagram of the sample (Al_2O_3 substrate and TiO_2/ZnO composite film from bottom to top).

sample was conducted four times of the degradation experiment at all. The tested sample was dried at 60 °C for 2 h and then laid aside at room temperature in the dark for 12 h before the next repeated test.

X-ray diffractometer (X'Pert PRO, PANalytical B.V.) was employed to analyze the crystal structures of all samples applying graphite monochromatic with Cu Kα1 radiation in the 2θ range from 20 to 80°. The morphology and grain size of the composite were observed through field emission scanning electron microscopy (FE-SEM, Hitachi S-4800). Optical properties of the material were characterized by UV–vis diffuse reflectance spectrophotometer (UV–vis DRS, Lambda 35, PerkinElmer) and photoluminescence spectrometer (PL, USB2000-FLG Ocean Optics spectrometer).

3. Results and discussion

3.1. Characterization of TiO_2/ZnO composite

X-ray diffraction (XRD) patterns for nanocomposites with different ingredient are shown in Fig. 2. The XRD peaks of the TiO_2 samples are in good agreement with the anatase structure TiO_2 (JCPDS 21-1272) and rutile structure TiO_2 (JCPDS 21-1276). The TiO_2 sample used in the experiment is calculated to consist of 80% anatase phase and 20% rutile phase by semi-quantitative estimate [39], which is consistent with the product information of TiO_2. The XRD peaks of the ZnO samples are in good agreement with the hexagonal wurtzite structure ZnO (JCPDS 36-1451). From Fig. 2, it can be observed that TiO_2 and ZnO are in good crystallization. The intensity of the XRD peaks demonstrates that the anatase and the rutile phase TiO_2 decreases with X_{ZnO} increasing from 0 to 1, while the ZnO phase increases (Fig. 2(B)). Herein, X_{ZnO} denotes the mole fraction of ZnO in TiO_2/ZnO composite.

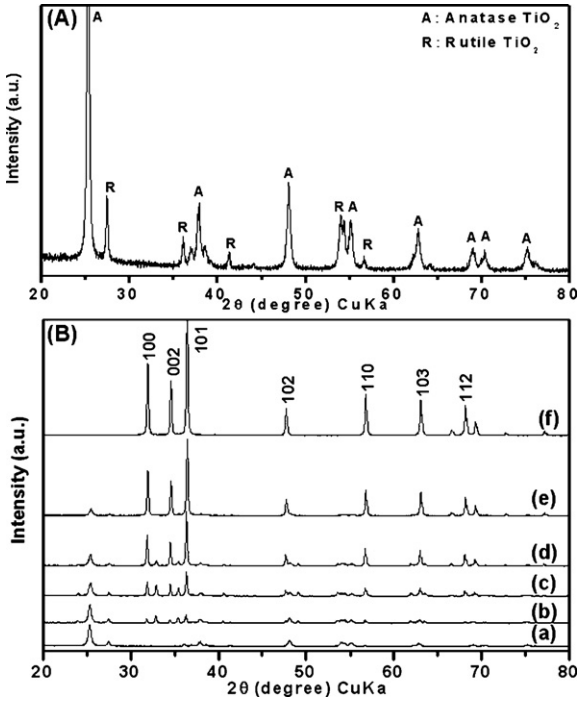

Fig. 2. X-ray diffraction (XRD) pattern of different ingredient points of TiO_2/ZnO composite: (a) TiO_2, (b) $X_{ZnO} = 0.2$ (TiO_2:ZnO = 8:2), (c) $X_{ZnO} = 0.4$ (TiO_2:ZnO = 6:4), (d) $X_{ZnO} = 0.6$ (TiO_2:ZnO = 4:6), (e) $X_{ZnO} = 0.8$ (TiO_2:ZnO = 2:8), (f) ZnO. X_{ZnO} denotes the mole fraction of ZnO in TiO_2/ZnO composite.

The SEM photographs of different ingredient points of TiO_2/ZnO composite are revealed in Fig. 3. It can be observed that

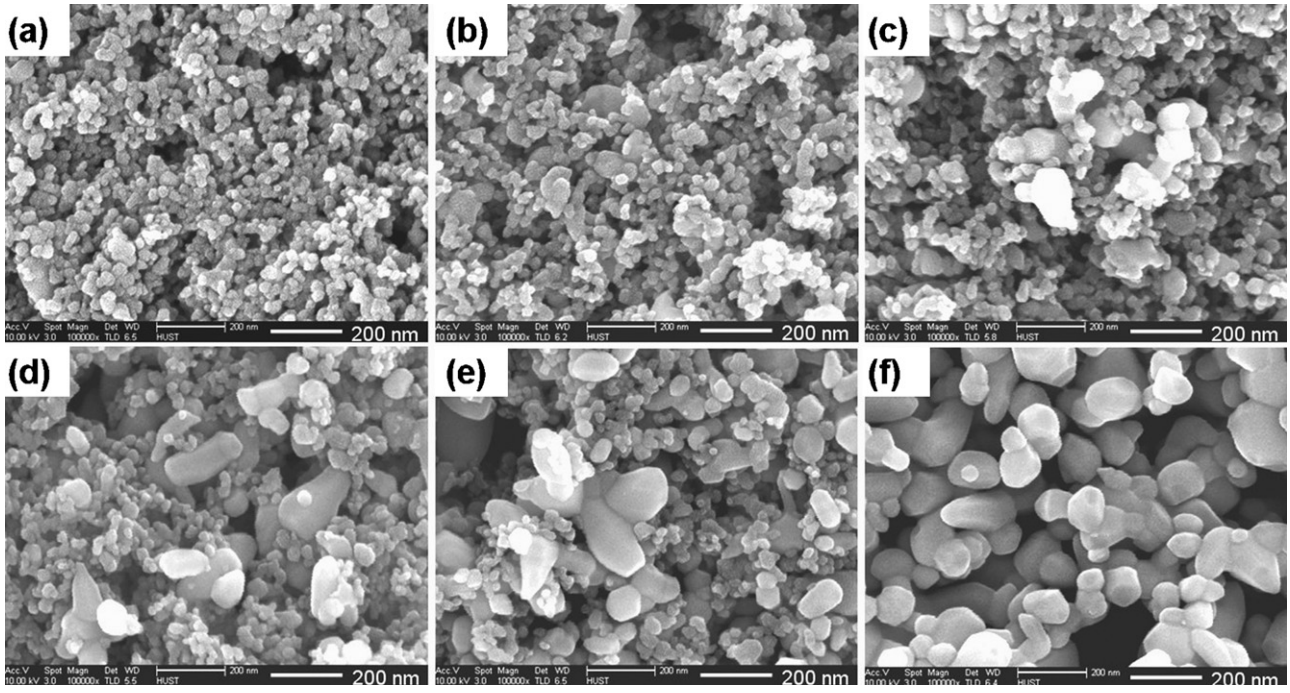

Fig. 3. SEM photographs of different ingredient points of TiO_2/ZnO composite: (a) TiO_2, (b) $X_{ZnO} = 0.2$ (TiO_2:ZnO = 8:2), (c) $X_{ZnO} = 0.4$ (TiO_2:ZnO = 6:4), (d) $X_{ZnO} = 0.6$ (TiO_2:ZnO = 4:6), (e) $X_{ZnO} = 0.8$ (TiO_2:ZnO = 2:8), (f) ZnO. X_{ZnO} denotes the mole fraction of ZnO in TiO_2/ZnO composite.

the TiO_2 particles are about 30 nm (Fig. 3(a)) and the ZnO particles are about 80 nm (Fig. 3(f)), all uniformly distributed with no obvious growth compared with as received raw material. There are no other phases observed in the SEM images of TiO_2 and ZnO. As shown in the SEM images, the number of TiO_2 particles decreases while the number of ZnO particles increases with X_{ZnO} increasing from 0 to 1. For ingredient point with $X_{ZnO} = 0.2$ and 0.4 (Fig. 3(b) and (c)), a small quantity of ZnO particles are distributed among the relatively numerous TiO_2 particles. As for ingredient point with $X_{ZnO} = 0.6$ and 0.8 (Fig. 3(d) and (e)), TiO_2 particles are distributed among ZnO particles.

The UV–vis diffuse reflectance spectra of TiO_2 and ZnO samples are displayed in Fig. 4. The TiO_2 and ZnO samples exhibit two absorptions below 400 nm and 387 nm, which correspond to their absorption edges ($E_g = 3.1$ eV for TiO_2 and $E_g = 3.2$ eV for ZnO), respectively. The Kubelkka–Mulk absorbance at 365 nm of ZnO is 40% higher than that of TiO_2, which means that the absorbability to UV light (365 ± 5 nm) of ZnO is better than that of TiO_2. The UV–vis spectra of TiO_2/ZnO composite display the common characteristic of TiO_2 and ZnO, while the Kubelkka–Mulk absorbance at 365 nm of TiO_2/ZnO composite is higher than that of TiO_2 and ZnO. Photoluminescence (PL) spectra of TiO_2 and ZnO under excitation at 300 nm are shown in Fig. 5. These PL results are consistent with previous publications [40–44]. There are three PL peaks of ZnO, and the first one corresponds to the intrinsic recombination of photoinduced charges from the conduction band to the valence band. PL peaks at 510 nm and 790 nm are the signals of the defect levels of ZnO. As an indirect wide-gap semiconductor, the band edge luminescence of TiO_2 is difficult to be observed [45]. Hence, there is only one PL peak at 500 nm which is corresponding to the defect level of TiO_2.

3.2. Photocatalytic properties of TiO_2, ZnO and their composite for formaldehyde degradation

Previous studies revealed that the photocatalytic degradation of formaldehyde was a pseudo-first-order reaction [4,46–48].

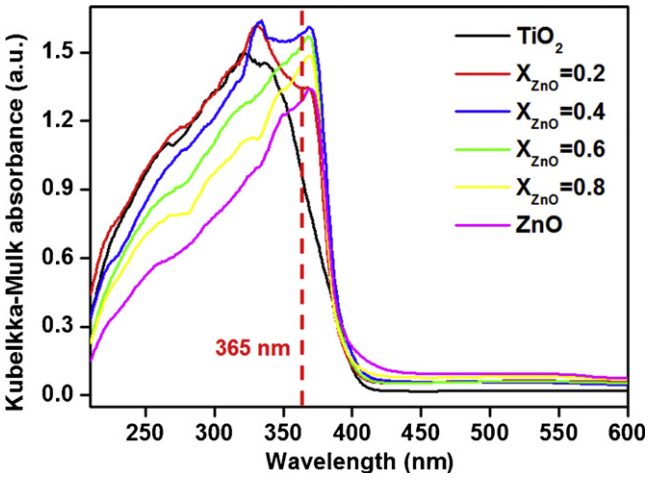

Fig. 4. UV–vis diffuses reflectance spectra of TiO_2/ZnO samples. X_{ZnO} denotes the mole fraction of ZnO in TiO_2/ZnO composite.

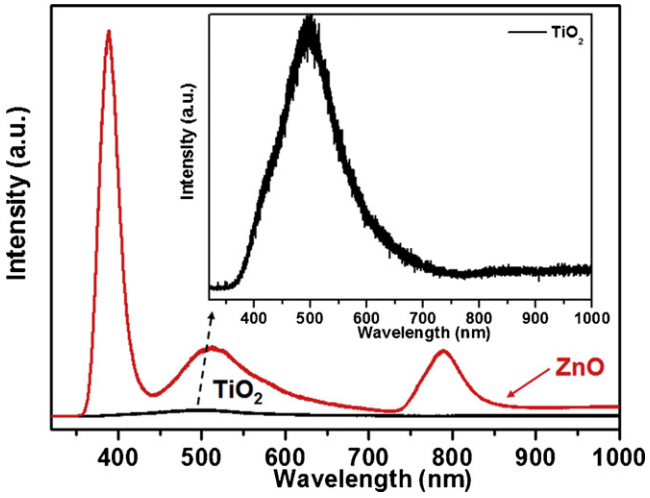

Fig. 5. Photoluminescence (PL) spectra of TiO_2 and ZnO.

The kinetic equation can be expressed as follows:

$$\frac{c_t}{c_0} = e^{-kt} \quad (1)$$

where k is the apparent rate constant, c_t is the concentration of formaldehyde at time t, and c_0 is the initial concentration of formaldehyde. Our degradation results are consistent with the above reaction. The photocatalytic properties of TiO_2/ZnO composite and their rate constants for formaldehyde degradation are shown in Fig. 6. The photocatalytic degradation does not take place in the absence of either photocatalysts or UV light, indicated by the blank data in Fig. 6. As can be seen, the photocatalytic property of TiO_2 for formaldehyde degradation is observed stable under our experimental treatment, and 50 ppm formaldehyde is degraded to 1 ppm within 60 min (Fig. 6(a)). The degradation rate constant of TiO_2 is 0.05 min^{-1} 1 fitted by formula (1) (Fig. 6(c)). In contrast, there is no significant degradation of formaldehyde by ZnO (Fig. 6(b)). The degradation rate constant of ZnO is 0.0006 min^{-1} (Fig. 6(c)). Obviously, the rate constant of TiO_2 is two orders of magnitude larger than that of ZnO under the same conditions.

Previously, Wang et al. compared the dye degradation efficiency using ZnO powders with various size scales, and found that the size was not the most important factor for the photocatalytic activity of ZnO nanoparticle [20]. According to their results we can make sure that the size differences between TiO_2 and ZnO is not the main reason which results in the very different photocatalytic properties of TiO_2 and ZnO. Generally speaking, after the absorption of reactants at the surface of the catalyst, the photocatalysis reaction in the absorbed phase involves photocatalytic physical and photocatalytic chemical process [49,50]. We try to explore the reason of the differences of photocatalytic properties between TiO_2 and ZnO from the viewpoint of photocatalytic physics and photocatalytic chemistry. Photocatalytic physics mainly contains two processes: (1) absorption of light, (2) the generation and recombination of photogenerated electrons and holes. Meanwhile, in photocatalytic chemistry, the driving force of electrons and holes transfer is a measure of the oxidoreduction

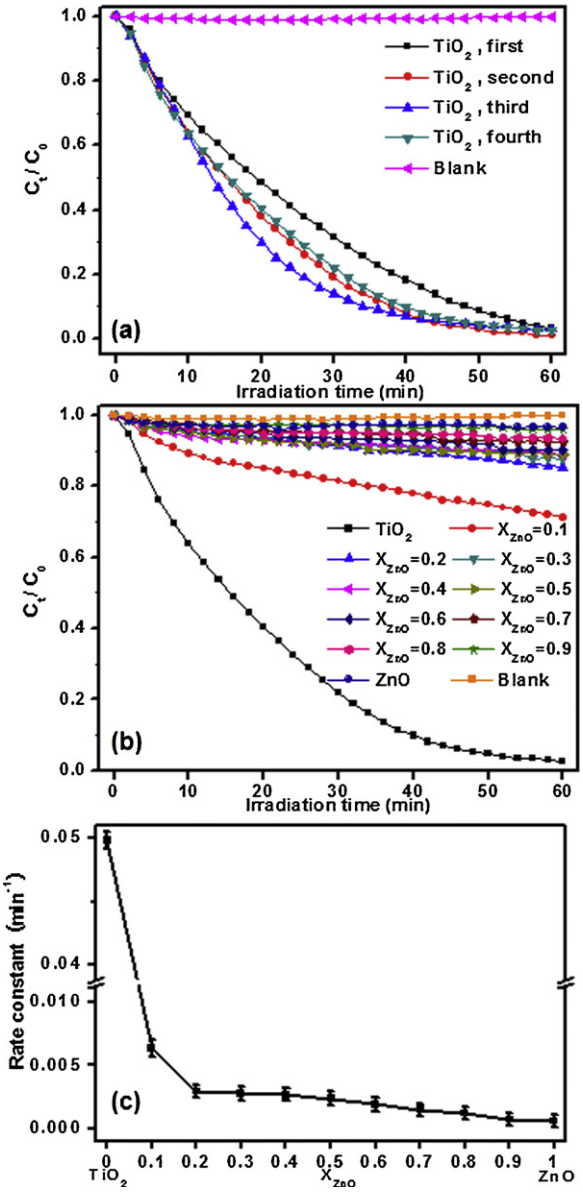

Fig. 6. Photocatalytic degradation of formaldehyde by TiO_2 (a) and TiO_2/ZnO composite (b) under ultraviolet LED (365 ± 5 nm, 3.6 mW/cm^2) illumination at room temperature (298 K). c_t is the concentration of formaldehyde at time t, and c_0 is the initial concentration of formaldehyde. Here we do not show the error bar in (b) because of the finite space. The rate constants of TiO_2/ZnO composite for formaldehyde degradation (c). X_{ZnO} denotes the mole fraction of ZnO in TiO_2/ZnO composite.

ability of photoinduced electrons and holes of the material. The driving force for organic degradation can be expressed as follows [6,51]:

$$\Delta E(e^-) = E_C - E_{LUMO} \quad (2)$$

$$\Delta E(h^+) = E_V - E_{HOMO} \quad (3)$$

where, $\Delta E(e^-)$ and $\Delta E(h^+)$ are the driving force of electrons transfer and holes transfer between the semiconductor catalyst and the organic molecules, respectively. E_C and E_V are the energy level of the conduction band and valence band of the semiconductor, respectively. E_{LUMO} and E_{HOMO} is the energy

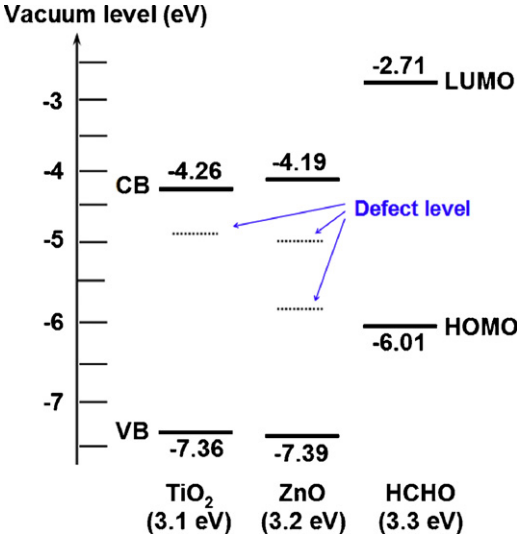

Fig. 7. Schematic diagram for the flat-band potentials of TiO_2, ZnO and HCHO.

level of the lowest unoccupied molecular orbital (LUMO) and the highest occupied molecular orbital (HOMO) of the organic molecules.

In terms of the calculating of the energy band structure of metal oxide semiconductor [17,40,41,43,44,46], combined with our characterization results of UV–vis and PL spectra, schematic diagram for the flat-band potentials of TiO_2, ZnO and HCHO is displayed in Fig. 7. According to formulae (2) and (3), the driving force of electrons and holes transfer between TiO_2 and HCHO are: $\Delta E(e^-, TiO_2) = 1.55$ eV and $\Delta E(h^+, TiO_2) = 1.35$ eV. The driving force of electrons and holes transfer between ZnO and HCHO are: $\Delta E(e^-, ZnO) = 1.48$ eV and $\Delta E(h^+, ZnO) = 1.38$ eV. Clearly, the differences of the driving forces of electrons and holes transfer between them are tiny. In other words, the oxidoreduction ability of photoinduced electrons and holes of TiO_2 for formaldehyde degradation is close to that of ZnO. Thus, there are few differences between TiO_2 and ZnO in photocatalytic chemistry, implying that photocatalytic chemistry has little influence on the differences of photocatalytic properties between ZnO and TiO_2. As photocatalysis process involves photocatalytic physical process and photocatalytic chemical process, the very inferior photocatalytic property of ZnO to TiO_2 may result from the differences of photocatalytic physical processes between them. Photocatalytic physical process contains absorption of light and the generation and recombination of photogenerated electrons and holes. From the aspect of the absorption of light, the absorbability to UV light (365 ± 5 nm) of ZnO is higher than that of TiO_2 (as shown in Fig. 4). In our previous work, it has been found that the photocurrent of ZnO was four orders of magnitude larger than that of TiO_2 under external electric field at the same conditions [39]. On the basis of the definition of IPCE (incident photon-to-electron conversion efficiency), the formula is given as below [52,53]:

$$IPCE = \frac{\Delta N_{electron}}{N_{photon}} \quad (4)$$

where, N_{photon} denotes the number of the incident photons, $\Delta N_{electron}$ denotes the number of the photogenerated electrons. Obviously, the IPCE of ZnO is larger than that of TiO_2 under the same conditions, which means that ZnO generates much more photoinduced charges than TiO_2. Therefore, the very inferior photocatalytic property of ZnO to TiO_2 may essentially come from the recombination of photoinduced charges. Fortunately, the radiative recombination of photoinduced charges can be reflected by photoluminescence (PL) signals [54,55]. In general, high PL intensity originates from large quantities of recombination of photoinduced electron–holes. It can be seen that the intensity of ZnO's PL peak is much larger than that of TiO_2. The first PL signal of interband (band-to-band) of ZnO is especially intensive (Fig. 5), which indicates that the recombination of photoinduced electrons and holes of ZnO is more excessive compared with TiO_2. Meanwhile, as well known, defect level close to the conduction band or valence band is shallow level that cannot play the effective role of recombination center. Nevertheless, the deeper level located in the center of forbidden band is the most effective recombination center. For TiO_2, the PL peak intensity of defect level is weak to some extent that displays the characteristic of the shallow level. As for ZnO, the two defect peaks are of little difference, both of which display the characteristic of the deep level. Thus, most photoinduced electrons and holes of ZnO may have recombined before they react with gaseous formaldehyde. Therefore, there are inadequate photoinduced electrons and holes to react with gaseous formaldehyde which results in the inferior photocatalytic property of ZnO. In addition, many studies have elaborated the eximious photocatalytic property of TiO_2 [56,57]. The stable charge separation by electron transfer from conduction band of rutile to that of anatase slows the recombination of photoinduced electrons and holes, which results in the eximious photocatalytic property of TiO_2 catalysts with mixed rutile and anatase phase [56]. All in all, the very inferior photocatalytic property of ZnO to that of TiO_2 may essentially result from the much excessive recombination of photoinduced charges of ZnO in the photocatalytic physical process. To obtain higher photocatalytic property of ZnO, the recombination of photoinduced charges needs to be suppressed. Relevant research will be carried out in the near future.

The photocatalytic properties of TiO_2/ZnO composite for formaldehyde degradation are far worse than TiO_2, while better than ZnO (Fig. 6(b) and (c)). The addition of a small amount of ZnO weakens the photocatalytic property of TiO_2. The more amount of ZnO, the more weakened effect it demonstrates. In order to clearly explore the photocatalysis effect of TiO_2/ZnO composite for formaldehyde degradation by quantitative analysis, we calculated the composition effect of TiO_2/ZnO composite according to our previous definition of composition effect (*CE*) [39]:

$$CE = \frac{k}{X_{TiO_2} \cdot k_{TiO_2} + X_{ZnO} \cdot k_{ZnO}} \quad (5)$$

where, k is the apparent rate constant of the composite. X_{TiO_2} and X_{ZnO} denote the mole fraction of TiO_2 and ZnO of the corresponding ingredient point in TiO_2/ZnO composite, respectively. k_{TiO_2} and k_{ZnO} represent the apparent rate constant of TiO_2 and ZnO under the same conditions, respectively. Here, if $0 < CE < 1$, the composite weakens the properties of the matrix. If $CE = 1$, the composite does not change the properties of the matrix obviously. If $CE > 1$, the composite enhances the properties of the matrix. As shown in Fig. 8, *CE* is much less than 1, thus the photocatalytic property of TiO_2 matrix was largely weakened. These results can also be explained from the two aspects of photocatalytic physics and photocatalytic chemistry. First, the driving force in the photocatalytic chemistry of TiO_2/ZnO composite will not be changed obviously compared to TiO_2 and ZnO, because of their slight differences in driving force of electrons and holes transfer. Second, the absorbability to UV light (365 ± 5 nm) of TiO_2/ZnO composite is better than that of TiO_2 and ZnO (Fig. 4). According to our previous work, the IPCE of some ingredient point of TiO_2/ZnO composite is larger than that of TiO_2 and ZnO under external electric field at the same conditions [39], which means some ingredient point of TiO_2/ZnO composite could generate more photoinduced charges than TiO_2 and ZnO alone. Therefore, the inferior photocatalytic properties of TiO_2/ZnO composite may mainly result from the differences of the recombination of photoinduced charges in the photocatalytic physical process. Some studies found that the transferring of photoinduced electrons and holes between the energy levels of TiO_2 and ZnO could achieve effective separation of photoinduced charges and reduce the recombination rate significantly within the TiO_2/ZnO composite, which consequently enhanced the photocatalytic properties of them in liquid [32,58]. However, on the basis of our results of the inferior photocatalytic properties of TiO_2/ZnO composite, we found that the separation effect of electrons and holes transfer between TiO_2 and ZnO was not being obvious in our experiment. This may be ascribed to that the recombination action of photoinduced electron–hole pairs in ZnO surpasses the charge separation of electrons and holes transfer between TiO_2 and ZnO. Therefore, the composition effect of TiO_2/ZnO composite for formaldehyde degradation is less than 1.

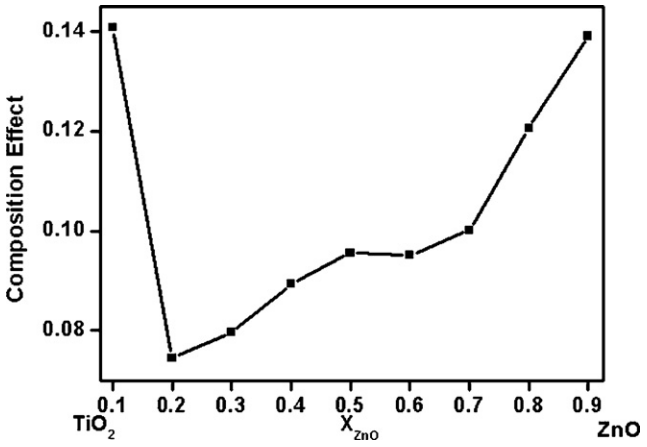

Fig. 8. The composition effect of TiO_2/ZnO composite for formaldehyde photocatalytic degradation. X_{ZnO} denotes the mole fraction of ZnO in TiO_2/ZnO composite.

4. Conclusion

The photocatalytic property of TiO_2 for formaldehyde degradation is stable under our experimental treatment, and 50 ppm formaldehyde is degraded to 1 ppm within 60 min. The degradation rate constant of TiO_2 is $0.05\ min^{-1}$. The photocatalytic property for formaldehyde degradation of ZnO is very inferior to TiO_2 under the same conditions. Through comprehensive analysis of UV–vis spectra, PL spectra, the energy band diagram and the photocatalytic properties of TiO_2 and ZnO, we consider that the differences of photocatalytic properties between ZnO and TiO_2 may essentially originate from the photocatalytic physical process, i.e., the recombination of photoinduced electrons and holes of ZnO.

The photocatalytic properties of TiO_2/ZnO composite for formaldehyde degradation are much worse than that of TiO_2 but better than that of ZnO. The addition of a small amount of ZnO weakens the photocatalytic property of TiO_2. The more amount of TiO_2, the weaker effect it demonstrates. The composition effect of TiO_2/ZnO composite for formaldehyde degradation is less than 1. This may be attributed to that the recombination action to photoinduced electron-hole pairs of ZnO surpasses the charge separation of electrons and holes transfer between TiO_2 and ZnO.

Acknowledgments

This work was supported by Nature Science Foundation of China (No. 50927201) and the National Basic Research Program of China (Grant Nos. 2009CB939705 and 2009CB939702). The authors are also grateful to Analytical and Testing Center of Huazhong University of Science and Technology.

References

[1] U.S. EPA, An Introduction to Indoor Air Quality-Organic Gases (Volatile Organic Compounds – VOCs), 2009.
[2] L.V. Bayless, Photocatalytic Oxidation of Volatile Organic Compounds for Indoor Air Applications, 2009.
[3] X. Zhang, Q.Q. Liu, Visible-light-induced degradation of formaldehyde over titania photocatalyst co-doped with nitrogen and nickel, Appl. Surf. Sci. 254 (2008) 4780–4785.
[4] R. Akbarzadeh, S.B. Umbarkar, R.S. Sonawane, S. Takle, M.K. Dongare, Vanadia–titania thin films for photocatalytic degradation of formaldehyde in sunlight, Appl. Catal. A: Gen. 374 (2010) 103–109.
[5] D.E. Huang, S.J. Liao, S.Q. Quan, L. Liu, Z.J. He, J.B. Wan, W.B. Zhou, Preparation and characterization of anatase N–F–codoped TiO_2 sol and its photocatalytic degradation for formaldehyde, J. Mater. Res. 22 (2007) 2389–2397.
[6] L. Ge, M.X. Xu, H.B. Fang, Photo-catalytic degradation of methyl orange and formaldehyde by Ag/$InVO_4$–TiO_2 thin films under visible-light irradiation, J. Mol. Catal. A: Chem. 258 (2006) 68–76.
[7] Y. Iguchi, H. Ichiura, T. Kitaoka, H. Tanaka, Preparation and characteristics of high performance paper containing titanium dioxide photocatalyst supported on inorganic fiber matrix, Chemosphere 53 (2003) 1193–1199.
[8] M.H. Habibi, M. Zendehdel, Synthesis and characterization of titania nanoparticles on the surface of microporous perlite using sol–gel method: influence of titania precursor on characteristics, J. Inorg. Organomet. Polym. 21 (2011) 634–639.
[9] K. Ubolchonlakate, L. Sikong, T. Tontai, Formaldehyde degradation by photocatalytic Ag-doped TiO_2 film of glass fiber roving, J. Nanosci. Nanotechnol. 10 (2010) 7522–7525.
[10] H. Yu, K. Zhang, C. Rossi, Experimental study of the photocatalytic degradation of formaldehyde in indoor air using a nano-particulate titanium dioxide photocatalyst, Indoor Built Environ. 16 (2007) 529–537.
[11] Y. Matsuo, Y. Nishino, T. Fukutsuka, Y. Sugie, Removal of formaldehyde from gas phase by silylated graphite oxide containing amino groups, Carbon 46 (2008) 1162–1163.
[12] L.F. Wang, M. Sakurai, H. Kameyama, Study of catalytic decomposition of formaldehyde on Pt/TiO_2 alumite catalyst at ambient temperature, J. Hazard. Mater. 167 (2009) 399–405.
[13] W.J. Liang, J. Li, Y.Q. Jin, Photo-catalytic degradation of gaseous formaldehyde by TiO_2/UV, Ag/TiO_2/UV and Ce/TiO_2/UV, Build. Environ. 51 (2012) 345–350.
[14] T.X. Liu, F.B. Li, X.Z. Li, TiO_2 hydrosols with high activity for photocatalytic degradation of formaldehyde in a gaseous phase, J. Hazard. Mater. 152 (2008) 347–355.
[15] R. Asahi, T. Morikawa, T. Ohwaki, K. Aoki, Y. Taga, Visible-light photocatalysis in nitrogen-doped titanium oxides, Science 293 (2001) 269–271.
[16] Y.X. Li, Y.A. Jiang, S.Q. Peng, F.Y. Jiang, Nitrogen-doped TiO_2 modified with NH_4F for efficient photocatalytic degradation of formaldehyde under blue light-emitting diodes, J. Hazard. Mater. 182 (2010) 90–96.
[17] Y. Xu, M.A.A. Schoonen, The absolute energy positions of conduction and valence bands of selected semiconducting minerals, Am. Mineral. 85 (2000) 543–556.
[18] Y.Z. Li, W. Xie, X.L. Hu, G.F. Shen, X. Zhou, Y. Xiang, X.J. Zhao, P.F. Fang, Comparison of dye photodegradation and its coupling with light-to-electricity conversion over TiO_2 and ZnO, Langmuir 26 (2010) 591–597.
[19] V. Kandavelu, H. Kastien, K.R. Thampi, Photocatalytic degradation of isothiazolin-3-ones in water and emulsion paints containing nanocrystalline TiO_2 and ZnO catalysts, Appl. Catal. B: Environ. 48 (2004) 101–111.
[20] H.H. Wang, C.S. Xie, W. Zhang, S.Z. Cai, Z.H. Yang, Y.H. Gui, Comparison of dye degradation efficiency using ZnO powders with various size scales, J. Hazard. Mater. 141 (2007) 645–652.
[21] H.H. Wang, C.S. Me, The effects of oxygen partial pressure on the microstructures and photocatalytic property of ZnO nanoparticles, Physica E 40 (2008) 2724–2729.
[22] H.H. Wang, C.S. Xie, Effect of annealing temperature on the microstructures and photocatalytic property of colloidal ZnO nanoparticles, J. Phys. Chem. Solids 69 (2008) 2440–2444.
[23] S.K. Kansal, M. Singh, D. Sud, Studies on TiO_2/ZnO photocatalysed degradation of lignin, J. Hazard. Mater. 153 (2008) 412–417.
[24] D.S. Bhatkhande, V.G. Pangarkar, A.A.C.M Beenackers, Photocatalytic degradation for environmental applications – a review, J. Chem. Technol. Biotechnol. 77 (2001) 102–116.
[25] M.H. Habibi, E. Askari, The effect of operational parameters on the photocatalytic degradation of C.I. Reactive Yellow 86 textile dye using manganese zinc oxide nanocomposite thin films, J. Adv. Oxid. Technol. 14 (2011) 190–195.
[26] M.A. Hasnat, M.M. Uddin, A.U. Samed, S.S. Alam, S. Hossain, Adsorption and photocatalytic decolorization of a synthetic dye erythrosine on anatase TiO_2 and ZnO surfaces, J. Hazard. Mater. 147 (2007) 471–477.
[27] M. Mrowetz, E. Selli, Photocatalytic degradation of formic and benzoic acids and hydrogen peroxide evolution in TiO_2 and ZnO water suspensions, J. Photochem. Photobiol. A 180 (2006) 15–22.
[28] S. Sakthivel, B. Neppolian, M.V. Shankar, B. Arabindoo, M. Palanichamy, V. Murugesan, Solar photocatalytic degradation of azo dye: comparison of photocatalytic efficiency of ZnO and TiO_2, Sol. Energy Mater. Sol. Cells 77 (2003) 65–82.
[29] E. Evgenidou, I. Konstantinou, K. Fytianos, I. Poulios, T. Albanis, Photocatalytic oxidation of methyl parathion over TiO_2 and ZnO suspensions, Catal. Today 124 (2007) 156–162.
[30] L.Q. Jing, B.F. Xin, F.L. Yuan, B.Q. Wang, K.Y. Shi, W.M. Cai, H.G. Fu, Deactivation and regeneration of ZnO and TiO_2 nanoparticles in the gas

phase photocatalytic oxidation of n-C_7H_{16} or SO_2, Appl. Catal. A: Gen. 275 (2004) 49–54.
[31] Y.Z. Lei, G.H. Zhao, M.C. Liu, Z.N. Zhang, X.L. Tong, T.C. Cao, Fabrication, characterization, and photoelectrocatalytic application of ZnO nanorods grafted on vertically aligned TiO_2 nanotubes, J. Phys. Chem. C 113 (2009) 19067–19076.
[32] Z.Y. He, Y.G. Li, Q.H. Zhang, H.Z. Wang, Capillary microchannel-based microreactors with highly durable ZnO/TiO_2 nanorod arrays for rapid, high efficiency and continuous-flow photocatalysis, Appl. Catal. B: Environ. 93 (2010) 376–382.
[33] M.H. Habibi, M. Mikhak, Synthesis of nanocrystalline zinc titanate ecandrewsite by sol–gel: optimization of heat treatment condition for red shift sensitization, Curr. Nanosci. 7 (2011) 603–607.
[34] X.T. Zhang, Y.A. Cao, S.H. Kan, Y.M. Chen, J. Tang, H.Y. Jin, Y.B. Bai, L.Z. Xiao, T.J. Li, B.F. Li, Study on the photo-induced interfacial charge transfer in TiO_2/Fe_2O_3 heterostructured composite film, Thin Solid Films 329 (1998) 568–570.
[35] B. Neppolian, Q. Wang, H. Yamashita, H. Choi, Synthesis and characterization of ZrO_2–TiO_2 binary oxide semiconductor nanoparticles: application and interparticle electron transfer process, Appl. Catal. A: Gen. 333 (2007) 264–271.
[36] G. Marci, V. Augugliaro, M.J. Lopez-Munoz, C. Martin, L. Palmisano, V. Rives, M. Schiavello, R.J.D. Tilley, A.M. Venezia, Preparation characterization and photocatalytic activity of polycrystalline ZnO/TiO_2 systems. 2. Surface, bulk characterization, and 4-nitrophenol photodegradation in liquid-solid regime, J. Phys. Chem. B 105 (2001) 1033–1040.
[37] R.L. Liu, H.Y. Ye, X.P. Xiong, H.Q. Liu, Fabrication of TiO_2/ZnO composite nanofibers by electrospinning and their photocatalytic property, Mater. Chem. Phys. 121 (2010) 432–439.
[38] Y. Liu, C.S. Xie, H.Y. Li, H. Chen, Y.C. Liao, D.W. Zeng, Low bias photoelectrocatalytic (PEC) performance for organic vapour degradation using TiO_2/WO_3 nanocomposite, Appl. Catal. B: Environ. 102 (2011) 157–162.
[39] Y.C. Liao, H.Y. Li, Y. Liu, Z.J. Zou, D.W. Zeng, C.S. Xie, Characterization of photoelectric properties and composition effect of TiO_2/ZnO/Fe_2O_3 composite by combinatorial methodology, J. Comb. Chem. 12 (2010) 883–889.
[40] X.L. Wang, Z.C. Feng, J.Y. Shi, G.Q. Jia, S.A. Shen, J. Zhou, C. Li, Trap states and carrier dynamics of TiO_2 studied by photoluminescence spectroscopy under weak excitation condition, Phys. Chem. Chem. Phys. 12 (2010) 7083–7090.
[41] P.L. Chen, X.Y. Ma, Y.Y. Zhang, D.S. Li, D.R. Yang, Electrophotoluminescence of sol-gel derived ZnO film: Effect of electric field on near-band-edge photoluminescence, Opt. Express 17 (2009) 11434–11439.
[42] J.M. Lin, H.Y. Lin, C.L. Cheng, Y.F. Chen, Giant enhancement of bandgap emission of ZnO nanorods by platinum nanoparticles, Nanotechnology 17 (2006) 4391–4394.
[43] H.B. Mao, K. Yu, J.Q. Wang, J.G. Yu, Z.Q. Zhu, Photoluminescence eigenmodes in a single ZnO nanobelt covering the ultraviolet and visible band, Opt. Express 17 (2009) 11860–11868.
[44] X.J. Wang, L.S. Vlasenko, S.J. Pearton, W.M. Chen, I.A. Buyanova, Oxygen and zinc vacancies in as-grown ZnO single crystals, J. Phys. D: Appl. Phys. 42 (2009) 175411.
[45] J. Shi, J. Chen, Z. Feng, T. Chen, Y. Lian, X. Wang, A.C. Li, Photoluminescence characteristics of TiO_2 and their relationship to the photoassisted reaction of water/methanol mixture, J. Phys. Chem. C 111 (2007) 693–699.
[46] J. Shang, S.D. Xie, T. Zhu, J. Li, Solid-state, planar photoelectrocatalytic devices using a manosized TiO_2 layer, Environ. Sci. Technol. 41 (2007) 7876–7880.
[47] H.M. Liu, Z.W. Lian, X.J. Ye, W.F. Shangguan, Kinetic analysis of photocatalytic oxidation of gas-phase formaldehyde over titanium dioxide, Chemosphere 60 (2005) 630–635.
[48] W.H. Ching, M. Leung, D.Y.C. Leung, Solar photocatalytic degradation of gaseous formaldehyde by sol–gel TiO_2 thin film for enhancement of indoor air quality, Sol. Energy 77 (2004) 129–135.
[49] J.M. Herrmann, Fundamentals and misconceptions in photocatalysis, J. Photochem. Photobiol. A 216 (2010) 85–93.
[50] J.M. Herrmann, Photocatalysis fundamentals revisited to avoid several misconceptions, Appl. Catal. B: Environ. 99 (2010) 461–468.
[51] S. Kerisit, K.M. Rosso, Charge transfer in FeO: a combined molecular-dynamics and ab initio study, J. Chem. Phys. 123 (2005) 224712.
[52] A.B. Murphy, P.R.F. Barnes, L.K. Randeniya, I.C. Plumb, I.E. Grey, M.D. Horne, J.A. Glasscock, Efficiency of solar water splitting using semiconductor electrodes, Int. J. Hydrogen Energy 31 (2006) 1999–2017.
[53] K. Hara, T. Horiguchi, T. Kinoshita, K. Sayama, H. Sugihara, H. Arakawa, Highly efficient photon-to-electron conversion with mercurochrome-sensitized nanoporous oxide semiconductor solar cells, Sol. Energy Mater. Sol. Cells 64 (2000) 115–134.
[54] W.S. Wang, L. Zhen, C.Y. Xu, W.Z. Shao, Room temperature synthesis, growth mechanism, photocatalytic and photoluminescence properties of cadmium molybdate core-shell microspheres, Cryst. Growth Des. 9 (2009) 1558–1568.
[55] W.F. Zhang, J.W. Tang, J.H. Ye, Photoluminescence and photocatalytic properties of $SrSnO_3$ perovskite, Chem. Phys. Lett. 418 (2006) 174–178.
[56] D.C. Hurum, A.G. Agrios, K.A. Gray, T. Rajh, M.C. Thurnauer, Explaining the enhanced photocatalytic activity of Degussa P25 mixed-phase TiO_2 using EPR, J. Phys. Chem. B 107 (2003) 4545–4549.
[57] H.K. Singh, M. Saquib, M.M. Haque, M. Muneer, Heterogeneous photocatalyzed degradation of uracil and 5-bromouracil in aqueous suspensions of titanium dioxide, J. Hazard. Mater. 142 (2007) 425–430.
[58] D. Chen, H. Zhang, S. Hu, J.H. Li, Preparation and enhanced photoelectrochemical performance of coupled bicomponent ZnO–TiO_2 nanocomposites, J. Phys. Chem. C 112 (2008) 117–122.